Journal of Molecular Modeling (2023) 29:328
https://doi.org/10.1007/s00894-023-05692-4

ORIGINAL PAPER

Examining O_2 adsorption on pristine and defective popgraphene sheets: A DFT study

David A. F. Martins[1] · Kleuton A. Lima[1] · Fábio F. Monteiro[2] · Marcelo L. Pereira Jr[3] · Luiz A. Ribeiro Jr[2] · Antonio Macedo-Filho[1]

Received: 22 March 2023 / Accepted: 11 August 2023 / Published online: 29 September 2023

Abstract

Context Popgraphene (PopG) is a two-dimensional carbon-based material with fused pentagonal and octagonal rings. Like graphene, it exhibits a metallic band gap and exceptional thermal, dynamic, and mechanical stability. Here, we theoretically study the electronic and structural properties of PopG monolayers, including their doped and vacancy-endowed versions, as O_2 adsorbers. Our findings show that pristine and vacancy-endowed PopG sheets have a comparable ability to adsorb O_2 molecules, with adsorption energies ranging from −0.57 to −0.59 eV (physisorption). In these cases, octagonal rings play a dominant role in the adsorption mechanism. Platinum and Silicon doping enhance the O_2 adsorption in areas close to the octagonal rings, resulting in adsorption energies ranging from −1.13 to −2.56 eV (chemisorption). Furthermore, we computed the recovery time for the adsorbed O_2 molecules. The results suggest that PopG/O_2 interaction in pristine and vacancy-endowed cases can change the PopG electronic properties before O_2 diffusion.

Methods Density Functional Theory (DFT) simulations, with Van der Waals corrections (DFT-D, within the Grimme scheme), were performed to study the structural and electronic properties of PopG/O_2 systems using the DMol3 code within the Biovia Materials Studio software. The exchange and correlation functions are treated within the generalized gradient approximation (GGA) as parameterized by Perdew-Burke-Ernzerhof (PBE) functional. We used the double-zeta plus polarization (DZP) for the basis set in these cases. We also considered the BSSE correction through the counterpoise method and the nuclei-valence electron interactions by including semi-core DFT pseudopotentials.

Keywords 2D materials · Carbon allotrope · O_2 Adsorption · Popgraphene · Density functional theory

Introduction

Carbon-based two-dimensional (2D) materials are an increasingly popular area of study in scientific and technological fields thanks to their remarkable thermal, mechanical, and dynamic stability [1]. This interest can be traced back to the discovery of graphene in 2004 [2] and its revolutionary impact on flat optoelectronics [3].

Theoretical predictions have identified several other noteworthy carbon-based 2D materials, such as penta-graphene [4], pha-graphene [5], ψ-graphene [6], and popgraphene (PopG) [7, 8]. In recent years, experimental successes in obtaining new 2D carbon-based materials have included biphenylene [9], γ-graphyne [10, 11], monolayer amorphous carbon [12], and 2D (C_{60}) fullerene network [13]. Numerous studies have shown that carbon-based materials can act as sensors and storage media for ions and small molecules [14–19].

PopG's porous topology makes it a suitable active layer for specific applications [7, 20, 21]. Density functional theory (DFT) and Molecular Dynamics (MD) simulations were conducted to investigate its hydrogen adsorption properties [20]. The results revealed that at 77 K, PopG has moderately higher H_2 gravimetric absorption than graphene. Furthermore, through analysis of the heats of adsorption and H_2

This paper belongs to the Topical Collection IX Symposium on Electronic Structure and Molecular Dynamics - IX SeedMol.

✉ Marcelo L. Pereira Jr
marcelo.lopes@unb.br

[1] Department of Physics, State University of Piauí, 64002-150 Teresina, Piauí, Brazil

[2] Institute of Physics, University of Brasilia, 70910-900 Brasília, Brazil

[3] University of Brasília, Faculty of Technology, Department of Electrical Engineering, 70910-900 Brasília, Brazil

density profiles near the carbon surface, it was found that PopG's superior absorption is primarily due to its higher surface area per carbon atom, making it geometrically favorable over graphene [20].

A separate DFT-based investigation also demonstrated the PopG surface's ability to adsorb H_2 [21]. The study explored PopG's hydrogen storage capacity in the presence of lithium-ion atoms trapped in the pentagonal rings of the PopG structure. The results indicated that a Li-decorated PopG sheet could bind up to four H_2 molecules per unit cell, with average adsorption energy between physisorption and atomic chemisorption. These properties suggest that reversible hydrogen storage at moderate temperatures and pressures could be possible [21]. The findings reported in the references [7, 20, 21] have sparked interest in investigating the capacity of PopG systems to adsorb and store O_2 molecules, a complex that has yet to be studied.

Incorporating dopants into the 2D carbon-based structures aims to harness their synergistic effects [22]. This procedure can further enhance the capture of small molecules compared to related pristine lattices [23]. Among the dopants usually considered in carbonaceous materials, platinum and silicon atoms stand out [24–27]. Pt possesses excellent catalytic properties and is widely known for its ability to facilitate oxygen-related reactions [28]. Several studies have demonstrated the efficacy of Pt in promoting oxygen adsorption and facilitating oxygen reduction reactions [28–30]. Si atoms, in turn, can introduce sp^3 hybridization into the carbon lattices [31, 32]. For instance, this alteration in the bond type configuration can enhance its reactivity towards oxygen, leading to improved oxygen capture efficiency [33]. In this way, the high reactivity and affinity for oxygen species in Pt-/Si-doped carbon-based materials make them attractive candidates for enhancing oxygen sensing and capture.

In this study, we employed DFT calculations to examine how O_2 adsorption affects the structural and electronic properties of PopG. Specifically, we investigated the impact of O_2 adsorption on Pt-doped, Si-doped, and vacancy-endowed PoPG monolayers. Pt and Si doping have been widely studied in carbon-based 2D materials for various purposes, including sensing and capturing of small molecules and multiple atoms [34–48].

Methodology

We employed DFT calculations, with Van der Waals corrections (DFT-D, within the Grimme scheme [49]) as implemented in the DMol3 code [50–52], to examine how O_2 adsorption affects the structural and electronic properties of pristine, doped, and vacancy-endowed PopG sheets. Our numerical approach considered the exchange-correlation generalized gradient approximation (GGA) functional, which takes into account the Perdew-Burle-Ernzerhof (PBE) functional [49, 53, 54] with unrestricted spin (DNP). A numerical basis set of atomic orbitals with polarized functions [55, 56] was also used. We considered the BSSE correction through the counterpoise method and the nuclei-valence electron interactions by including semi-core DFT pseudopotentials [57].

A $5 \times 5 \times 1$ Monkhorst-Park k-point mesh in the Brillouin zone [58] was adopted to optimize the system's geometry. We performed several convergence tests for k-point meshes, vacuum region separation, and energy cutoff (results not shown here). Based on these tests, we determined the following parameters to use: a self-consistent field (SCF) tolerance of 1×10^{-5} eV/atom, a maximum force on each atom of 0.002 Ha/Å, a maximum displacement of 0.005 Å, cutoff energy of 450 eV, and $2 \times 1 \times 1$ lattices with a vacuum spacing of 30 Å to avoid interactions between layer images. These parameters have been previously employed to study small molecule

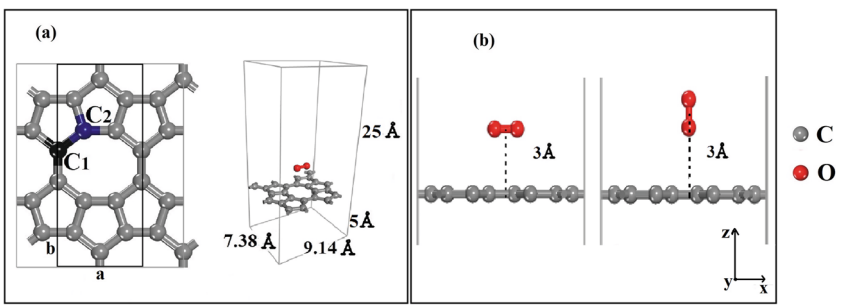

Fig. 1 The initial configuration of the simulations is schematically represented as follows: **a** the left panel shows a top view of the PopG monolayer, while the right panel shows a side view of the complete system; **b** the left and right panels depict the horizontal (H) and vertical (V) orientations of the O_2 molecule concerning the PopG monolayer. The red and grey spheres represent the carbon and oxygen atoms, respectively, and the grey sticks denote the C-C bonds

adsorption on nanostructured surfaces with successful results [59–63].

Figure 1 shows the starting configuration for all the cases studied here. The following abbreviations were adopted to refer to each case: PopG@O_2-(H,V), PopG-C_1/Pt@O_2-(H,V), PopG-C_2/Si@O_2-(H,V), and PopG-DEF@O_2-(H,V). Here, H and V refer to the horizontal and vertical alignments of O_2 concerning the PopG plane. The left panel in Fig. 1a shows a top view of the PopG sheet, with carbon atoms labeled as C_1 (black) and C_2 (blue). These carbon atoms are either replaced with Pt and Si or removed to create a vacancy.

There are many sites where the dopants can be placed in the PopG lattice. For including a dopant atom and a vacancy in this system, we chose the lattice site pointed as the most reactive one in reference [20]. Due to the significant computational costs involved, we have decided to refrain from performing this study regarding the multiple oxygen orientations on the popgraphene surface. To mitigate this limitation, we studied the vertical and horizontal orientations of the oxygen on the popgraphene surface. Moreover, We specifically focused on the triplet state of oxygen to evaluate the PopG capacity to absorb/capture O_2.

In Fig. 1a, the black rectangle highlights the PopG unit cell, while the right panel shows the overall system configuration and lattice dimensions. Figure 1b shows the initial positions of the O_2 molecule, with the left and right panels indicating the horizontal (H) and vertical (V) orientations of the molecule concerning the PopG monolayer. The molecule is placed 3.0 Å above the PopG plane in both cases. Note that the PopG lattice is positioned 5Å above the bottom of the simulation box.

The PopG structure consists of 12 atoms in its unit cell, with the $P2mg$ (group no.7) plane group and lattice parameters $a = 3.68$ Å and $b = 9.11$ Å. The carbon atoms occupy two non-equivalent atomic Wyckoff positions labeled C_1 and C_2 [7]. The bond lengths $C_1 - C_1$, $C_1 - C_2$, and $C_2 - C_2$ are 1.41 Å, 1.44 Å, and 1.46 Å, respectively. The left panel of Fig. 1a shows the $2 \times 2 \times 1$ supercell with lattice parameters $a = 7.38$ Å, $b = 9.14$ Å, and $c = 30.00$ Å used in the simulations. The lattice angles are $\alpha = \beta = \gamma = 90.00°$.

Results

To begin our discussion, we present the optimized configurations for all PopG@O_2 systems investigated in this study. Figure 2a and b show the results obtained for the pristine cases PopG@O2-V and PopG@O2-H, respectively. The adsorption energy E_{ads} was calculated using the expression $E_{ads} = E_{(PopG+O_2)} - E_{PopG} - E_{O_2}$, where E_{PopG}, E_{O_2}, and $E_{(PopG+O_2)}$ represent the total energies for isolated PopG, isolated O_2, and O_2 adsorbed on the PopG surface, respectively.

In both cases, the O_2 molecule was displaced from its initial position, with adsorption distances of $d = 3.03$ Å and $d = 3.22$ Å for PopG@O_2-V (Fig. 2a) and PopG@O2-H (Fig. 2b), respectively. The adsorption energies in the pristine cases are similar, with Eads $= -0.58$ eV for PopG@O2-V and Eads $= -0.59$ eV for PopG@O_2-H. These adsorption energies and distances indicate a physisorption mechanism. Notably, the O_2 molecule was adsorbed in the center of the octagonal ring, suggesting that O_2 adsorption in pristine PopG is orientation-independent.

Figure 3 displays the results of the geometry optimization for a PopG monolayer doped with a platinum atom. Specifically, Fig. 3a, b, c, and d depict the optimization results for PopG-C_1/Pt@O_2-H, PopG-C_2/Pt@O_2-H, PopG-C_1/Pt@O_2-V, and PopG-C_2/Pt@O_2-V, respectively. The labels C_1/Pt and C_2/Pt indicate that the platinum dopant has replaced the C_1 and C_2 atoms (see Fig. 1). The same color code used in Fig. 2 is adopted, with the addition of yellow spheres to represent platinum atoms. The red rectangle highlights the configuration with the lowest adsorption energy. The calculated adsorption energies are -1.86 eV (PopG-C_1/Pt@O_2-H), -1.13 eV (PopG-C_2/Pt@O_2-H), -1.85 eV (PopG-C_1/Pt@O_2-V), and -1.70 eV (PopG-C_2/Pt@O_2-V).

The dependence of E_{ads} on the orientation of the O_2 molecule is relatively small for the PopG-C_1/Pt@O_2-H (Fig. 3a) and PopG-C_1/Pt@O_2-V (Fig. 3c) cases. However, in the PopG-C_2/Pt@O_2-H and PopG-C_2/Pt@O_2-V cases (see Fig. 3b and d), the O_2 orientation and the Pt doping at the C_2 position can change the adsorption trend. This other adsorption pathway reduces the adsorption energy compared to the cases shown in Fig. 3a, c. Later on, we will show that the

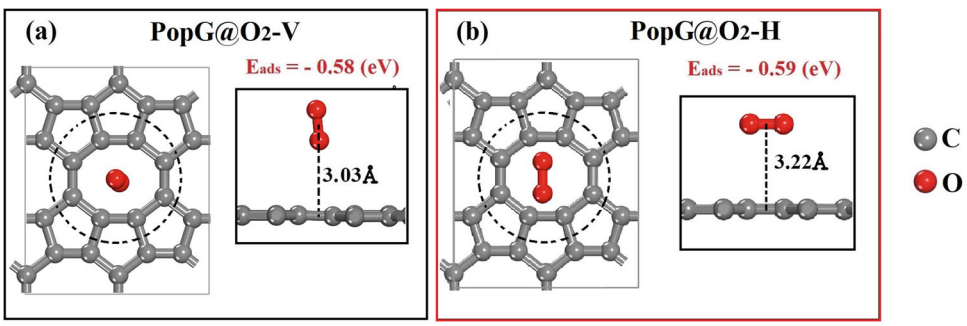

Fig. 2 The optimized configuration for pristine cases is schematically represented in **a** for PopG@O_2-V and in **b** for PopG@O_2-H. In the color code, red and grey spheres represent oxygen and carbon atoms. Grey sticks denote the C-C bonds. The configuration with lower adsorption energy is highlighted with a red rectangle

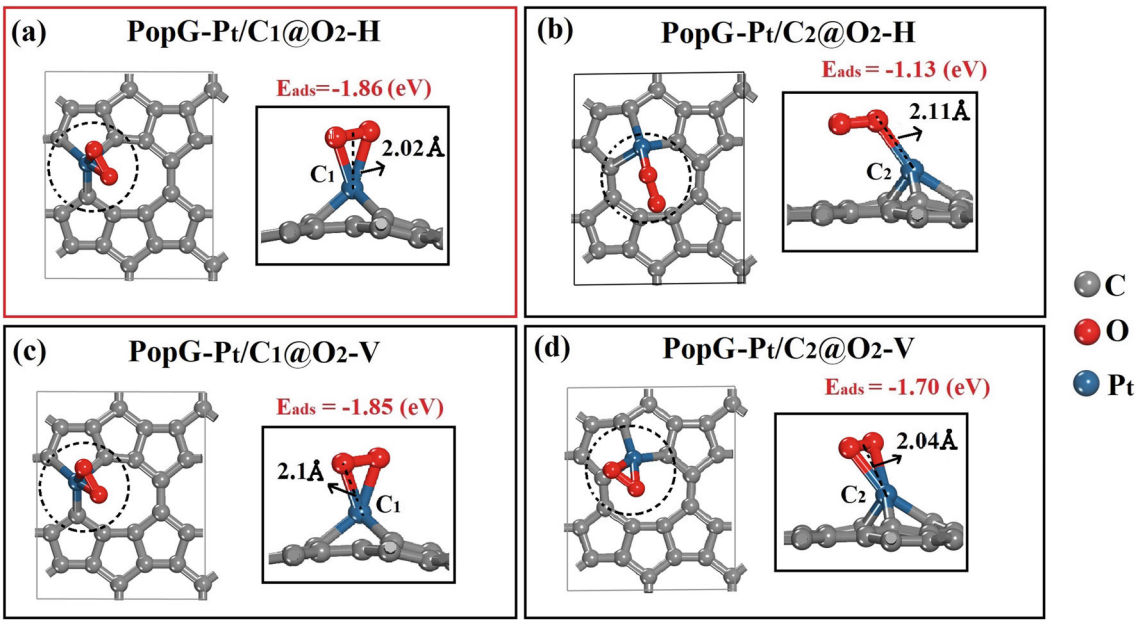

Fig. 3 The optimized configurations for platinum-doped cases, namely PopG-C_1/Pt@O_2-H, PopG-C_2/Pt@O_2-H, PopG-C_1/Pt@O_2-V, and PopG-C_2/Pt@O_2-V, are schematically represented in (**a**–**d**). The color code in the figure denotes oxygen, carbon, and platinum atoms with red, grey, and blue spheres, respectively. The grey sticks show the C-C bonds, while a red rectangle highlights the configuration with the lowest adsorption energy

adsorption energies tend to be lower in the center of the octagonal rings of PopG.

The adsorption distances are $d = 2.02$ Å, $d = 2.11$ Å, $d = 2.10$ Å, and $d = 2.04$ Å for the PopG-C_1/Pt@O_2-H, PopG-C_2/Pt@O_2-H, PopG-C_1/Pt@O_2-V, and PopG-C_2/Pt@O_2-V cases, respectively. The final O_2 configurations can present angles between 0-90 concerning the a-axis. Generally, the adsorption distances (Pt-O bond distances in these cases) are independent of the initial O_2 and doping configurations. These results indicate that the dopant dominates the adsorption mechanism. The adsorption energies and distances obtained for the Pt-doped PopG when interacting with O_2 indicate a chemisorption mechanism.

The results of the geometry optimization for PopG-C_1/Si@O_2-H, PopG-C_2/Si@O_2-H, PopG-C_1/Si@O_2-V, and PopG-C_2/Si@O_2-V are shown in Fig. 4a–d, following a similar approach to the cases discussed earlier. The labels C_1/Si and C_2/Si indicate that the silicon dopant replaces the C_1 and C_2 atoms (refer to Fig. 1). The color code used is the same as in Fig. 3, except for silicon atoms represented by yellow spheres. The red rectangle highlights the configuration with the lowest adsorption energy. The calculated adsorption energies are −2.38 eV (PopG-C_1/Si@O_2-H), −2.50 eV (PopG-C_2/Si@O_2-H), −2.26 eV (PopG-C_1/Si@O_2-V), and −2.52 eV (PopG-C_2/Si@O_2-V). As previously observed, the adsorption energies tend not to depend on the O_2 molecule orientation for the same lattice configurations, as depicted in Fig. 4a, c and b, d.

In contrast to what was observed in the pristine case, the O_2 molecule tends to be positioned nearly horizontally concerning the PopG surface in the case of silicon-doped PopG. The final O_2 configurations can have angles between 0 and 90 degrees for the a-axis, and the adsorption distances are $d = 1.59$ Å, $d = 1.57$ Å, $d = 1.60$ Å, and $d = 1.58$ Å for the PopG-C_1/Si@O_2-H, PopG-C_2/Si@O_2-H, PopG-C_1/Si@O_2-V, and PopG-C_2/Si@O_2-V cases, respectively. Generally, the adsorption distances (Si-O bond distances in these cases) are also independent of the initial O_2 and doping configurations. As previously noted for Pt-doped PopG cases, these results suggest that the dopant dominates the adsorption mechanism. The adsorption energies and distances obtained for the Si-doped PopG interacting with O_2 suggest a chemisorption mechanism.

Figure 5 illustrates the O_2 adsorption mechanism in vacancy-endowed (PopG-DEF) lattices. In Fig. 5a and b, we present the cases where the vacancy was generated by removing the C_2 atom (see Fig. 1), and the O_2 molecule was placed horizontally and vertically relative to the PopG monolayer, respectively. Since the C_1 vacancy results are similar, we show only the C_2 vacancy case. The calculated adsorption energies for both cases are about −0.57 eV. The adsorption distances are $d = 2.52$ Å and $d = 2.91$ Å for PopG-DEF@O_2-H (Fig. 5a) and PopG-DEF@O_2-V (Fig. 5b), respectively. The O_2 orientation on the PopG surface is also similar for these cases. These features suggest that the vacancy region dominates the adsorption mechanism.

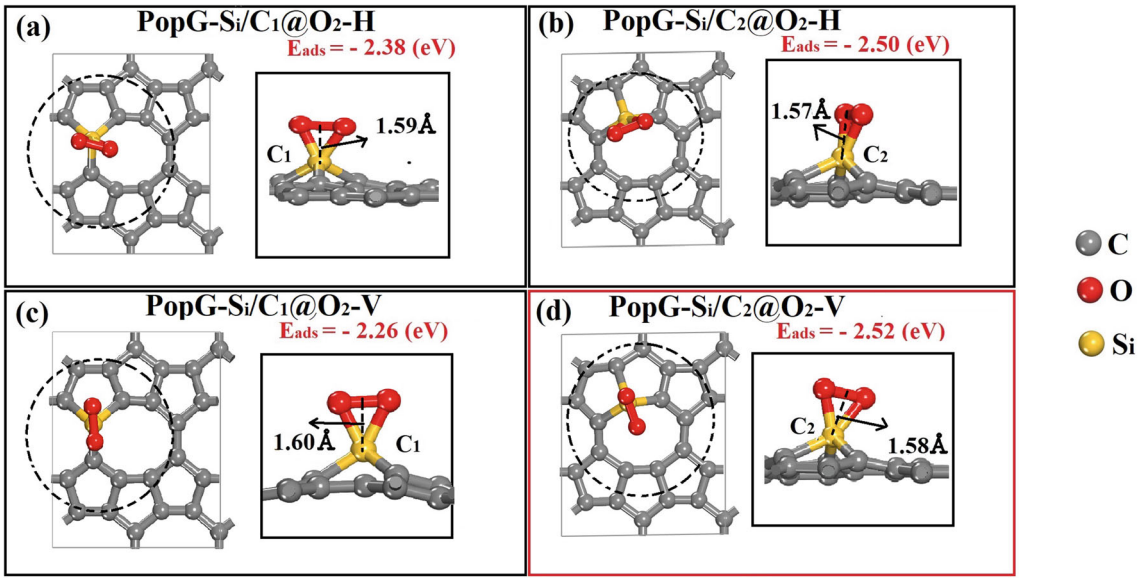

Fig. 4 **a**–**d** show schematic representations of the optimized configurations for the silicon-doped cases: PopG-C_1/Si@O_2-H, PopG-C_2/Si@O_2-H, PopG-C_1/Si@O_2-V, and PopG-C_2/Si@O_2-V, respectively. In the color code, oxygen, carbon, and silicon atoms are represented by red, grey, and yellow spheres, respectively, while the C-C bonds are shown as grey sticks. A red rectangle highlights the configuration with the lowest adsorption energy

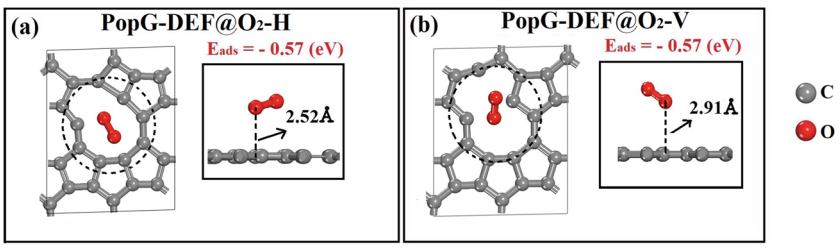

Fig. 5 **a** and **b** show schematic representations of the optimized configurations for the vacancy-doped cases: PopG-DEF/@O_2-H and PopG-DEF@O_2-V, respectively. In the color code used, oxygen and carbon atoms are represented by red and grey, respectively, while the C-C bonds are depicted as grey sticks

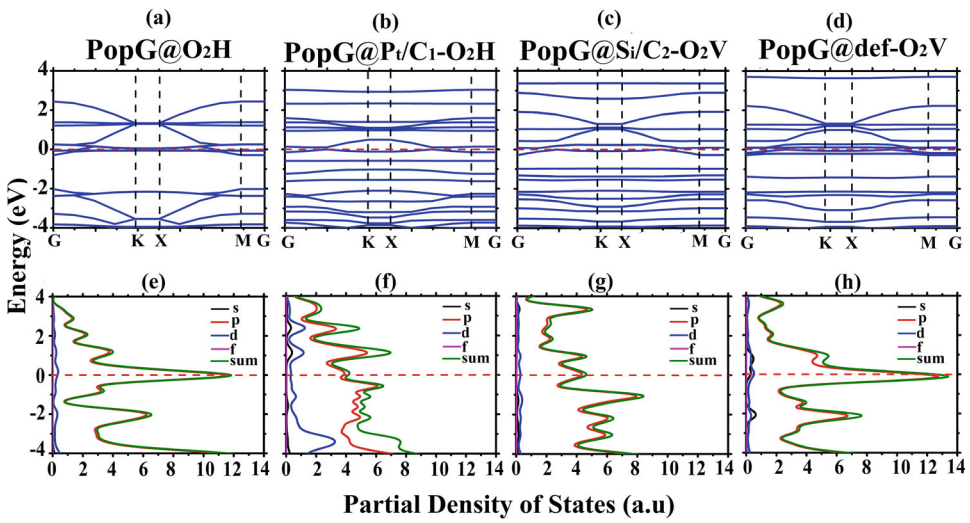

Fig. 6 The electronic band structure and its related projected density of states (PDOS) are displayed for the following cases: **a** PopG@O_2-H, **b** PopG-C_1/Pt@O_2-H, **c** PopG-C_2/Si@O_2-V, and **d** PopG-DEF@O_2-V. The valence atomic orbitals considered in each case are indicated on the panel label, and a dashed red line represents the Fermi level

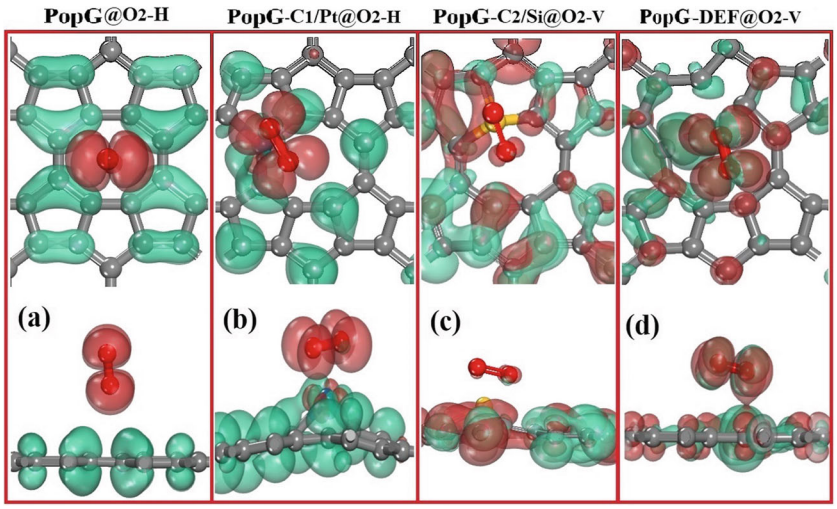

Fig. 7 Schematic representation of the charge spatial distribution of the HOMO and LUMO for the four cases: **a** PopG@O_2-H, **b** PopG-C_1/Pt@O_2-H, **c** PopG-C_2/Si@O_2-V, and **d** PopG-DEF@O_2-V. The color scheme uses green and red to represent HOMO and LUMO, respectively, while silver depicts the carbon atoms/carbon-carbon bonds. The red rectangles in this figure show all the cases with smaller adsorption energies

Moreover, these adsorption energies and distances indicate a physisorption mechanism.

Now, we discuss the electronic properties of the model PopG/O_2 cases with lower adsorption energies. Figure 6 displays the electronic band structure and projected density of states (PDOS) for four cases: PopG@O_2-H (Fig. 6a, e), PopG-C_1/Pt@O_2-H (Fig. 6b, f), PopG-C_2/Si@O_2-V (Fig. 6c, g), and PopG-DEF@O_2-V (Fig. 6d, h). The previous pristine and defective PopG studies can be found in references [7, 64]. Doped and vacancy-endowed PopG exhibit a bandgap opening of approximately 100 meV. As expected, the adsorption, doping, and vacancy perturbations introduce flat intraband levels. In the case of PopG@O_2-H, these flat levels occur within the conduction band due to O_2 adsorption (see Fig. 6a). In contrast, the doped and vacancy-endowed cases feature flat intraband levels in valence and conduction bands, as shown in Fig. 6b–d.

According to reference, [7], the general band profile of pristine PopG is not affected by defects or adsorption. The flat intraband levels observed in the band structure of PopG@O_2-H, PopG-C_1/Pt@O_2-H, and PopG-C_2/Si@O_2-V are attributed to *d* (blue) and *f* (pink) valence atomic orbitals, as shown in Fig. 6e, f, and g, respectively. In the PopG-C_1/Pt@O_2-H case, the flat levels are mainly due to the *d* orbital, as depicted in Fig. 6f. For PopG-DEF@O_2-V, the flat intraband levels near the Fermi level arise from the dangling bonds in the vicinity of the defect, leading to flat *p* levels (see Fig. 6h).

Figure 7 illustrates the localization of the Highest Occupied Molecular Orbital (HOMO) and Lowest Unoccupied Molecular Orbital (LUMO), also only for cases with lower adsorption energies. Generally, HOCO is distributed over PopG, while LUMO tends to be localized on O_2, as shown in Fig. 7a, b, and d. In the doped case of PopG-C_1/Pt@O_2-H (Fig. 7b), a small portion of LUMO is distributed over PopG, indicating a slight charge transfer from O_2 to PopG. In the case with higher charge transfer, PopG-C_2/Si@O_2-V (Fig. 7c), LUMO tends to be localized over PopG. For the defective case of PopG-DEF@O_2-V, HOMO and LUMO can be found over PopG and O_2, as depicted in Fig. 7d. In this delocalized pattern, a portion of LUMO is distributed over O_2 and PopG, greatly enhancing their interaction when compared to the pristine case of PopG@O_2-H (Fig. 7a).

To extend the description of the O_2 adsorption capability of pristine, doped, and vacancy-endowed PopG, we present in Fig. 8 adsorption energy maps for the minimum energy con-

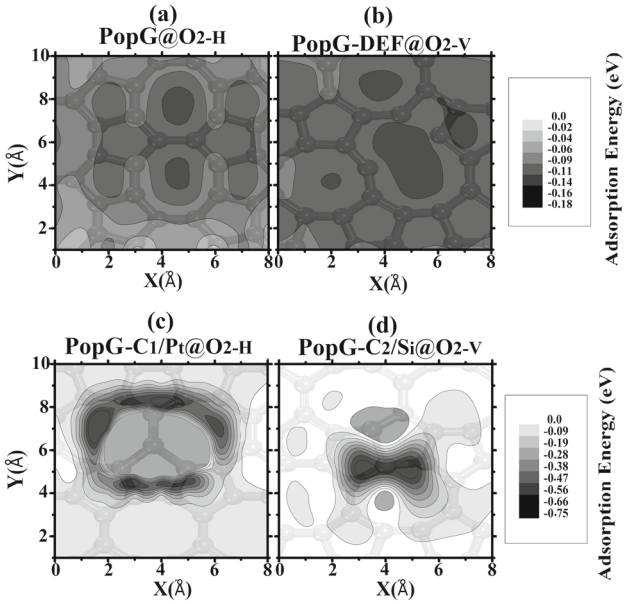

Fig. 8 This figure shows adsorption energy maps for four cases: **a** PopG@O_2-H, **b** PopG-DEF@O_2-V, **c** PopG-C_1/Pt@O_2-H, and **d** PopG-C_1/Si@O_2-V. The colors indicate the adsorption energy values, with black and white representing higher and lower values, respectively

figurations discussed above. The color scheme in this figure indicates adsorption energies, with higher and lower values represented by black and white colors, respectively. To construct these maps, we fixed the molecule's z-position (at 3.0 Å) and varied its x and y positions (with a 0.5 Å step) between 0–8 and 0–10 Å, respectively, on the PopG surface. These intervals were chosen to centralize the defects in the maps. As shown in Fig. 8a, in the pristine and vacancy-endowed cases (refer to Figs. 8a, b), the PopG regions with lower adsorption energies are those at the center of the octagons, pentagons, and vacancy, with adsorption energies varying from −0.04 to −0.18 eV. In contrast, in the doped cases, the lower interaction energies are found within and around the defective regions, as shown in Fig. 8c and d for the PopG-C_1/Pt@O_2-H, PopG-C_2/Si@O_2-V cases, respectively. In these cases, the adsorption energies vary from −0.09 to −0.75 eV.

It is worth mentioning that the electronic properties of pristine PopG demonstrate sensitivity to O_2 adsorption, similar to graphene [46]. However, when doped with Pt and Si, PopG and graphene [35, 45] exhibit increased reactivity towards O_2 adsorption. The presence of Pt in doped graphene induces local gas molecule polarization upon O_2 adsorption [45]. Interestingly, this polarization trend was not observed in the case of PopG. Regarding vacancy-endowed lattices, both PopG and graphene [65] exhibit strong interactions with O_2 molecules within the vacancy region. Furthermore, their metallic behavior is characterized by a large density of states near the Fermi level, indicating enhanced conductivity.

Generally, increasing the concentration of dopants with metal atoms in 2D carbon-based materials can lead to a substantial increase in the adsorption energies and the capacity to capture a higher number of small molecules. This phenomenon is primarily attributed to two key factors: electronic doping and the creation of active sites. The Supplementary Material shows the PopG-Pt and PopG-Si lattice structures upon doping with four metal atoms. Moreover, the number of O_2 molecules was also increased.

Finally, Table 1 summarizes the values obtained for the adsorption energies and distances, along with the recovery time (τ) [66] and charge transfer values. τ is the transient time for the molecule adsorption, with systems having higher τ values indicating better adsorption performance. The recovery time is calculated using the formula $\tau = \nu^{-1} \times \exp(-E_{ads}/k_B T)$, where ν is the molecule oscillation frequency ($10^{12}\ s^{-1}$ [67]), k_B is the Boltzmann constant, and T is the temperature (298 K). In Table 1, it can be observed that τ and Q_t are directly proportional to E_{ads}. For the systems that showed chemisorption, τ was not calculated. In this sense, the system with a higher recovery time is PopG@O_2 (about 9.50×10^{-3} s). However, all the recovery times for the pristine and vacancy-endowed cases are in the same order of magnitude (10^{-3} s, refer to Table 1). The τ values are large enough to facilitate the PopG/O_2 interaction, which can alter the PopG electronic properties discussed above before O_2 diffusion.

Table 1 This table summarizes the calculations for adsorption energies (E_{ads} in eV), recovery time (τ in seconds), equilibrium distance (d in Å), and charge transfer (Q_t) of O_2 adsorption on pristine, doped, and vacancy-endowed PopG monolayers

Structures	E_{ads} (eV)	τ (s)	d (Å)	Q_t (e)
PopG@O_2-H	−0.59	9.50×10^{-3}	3.22	−0.11
PopG@O_2-V	−0.58	6.40×10^{-3}	3.03	−0.11
PopG@Pt/C_1-O_2-H	−1.86	—	2.02	−0.45
PopG@Pt/C_1-O_2-V	−1.85	—	2.11	−0.45
PopG@Pt/C_2-O_2-H	−1.13	—	2.10	−0.33
PopG@Pt/C_2-O_2-V	−1.70	—	2.04	−0.42
PopG@Si/C_1-O_2-H	−2.38	—	1.59	−0.70
PopG@Si/C_1-O_2-V	−2.26	—	1.57	−0.70
PopG@Si/C_2-O_2-H	−2.52	—	1.60	−0.71
PopG@Si/C_2-O_2-V	−2.50	—	1.58	−0.70
PopG-DEF@O_2-H	−0.57	4.40×10^{-3}	2.52	−0.10
PopG-DEF@O_2-V	−0.57	4.40×10^{-3}	2.91	−0.11

Conclusions

In summary, we employed DFT calculations to examine how O_2 adsorption affects the structural and electronic properties of PopG. We investigated the impact of O_2 adsorption on Pt-doped, Si-doped, and vacancy-endowed PoPG monolayers. Generally, our findings revealed that O_2 could undergo physisorption (in pristine and vacancy-endowed monolayers) or chemisorption (in doped monolayers), which can alter the electronic properties of PopG.

The adsorption energies for both pristine and vacancy-endowed cases are approximately −0.58 eV. In the pristine and defective cases, the O_2 molecule was adsorbed in the center of the octagonal ring and the vacancy region, respectively. This trend implies that O_2 adsorption is not dependent on orientation in these PopG structures. These observations suggest that the octagonal ring and the vacancy region significantly influence their respective adsorption mechanisms. Furthermore, these cases' adsorption energies and distances indicate a physisorption mechanism.

In the (Pt,Si)-doped cases, the presence of a dopant dominates the adsorption mechanism. The adsorption energies and distances obtained for the (Pt,Si)-doped PopG when interacting with O_2 indicate a chemisorption mechanism.

Doped and vacancy-endowed PopG exhibit a bandgap opening of approximately 100 meV. As expected, the adsorption, doping, and vacancy perturbations introduce flat intraband levels. In the pristine cases, these flat levels occur within

the conduction band due to O_2 adsorption. In contrast, the doped and vacancy-endowed cases feature flat intraband levels in valence and conduction bands.

We also determined the recovery time for the adsorbed O_2 molecules. Our results suggest that PopG's electronic properties can be influenced by its interaction with O_2 in pristine and vacancy-endowed cases before O_2 diffusion.

Supplementary Information The online version contains supplementary material available at https://doi.org/10.1007/s00894-023-05692-4.

Acknowledgements L.A.R.J acknowledges the financial support from Brazilian Research Council FAP-DF grants 00193 − 00001247/2021 − 20, 00193 − 00000811/2021 − 97, and 00193 − 00000857/2021 − 14, CNPq grants 302236/2018 − 0 and 350176/2022 − 1, and FAPDF-PRONEM grant 00193.00001247/2021 − 20. F.F.M acknowledges the financial support from FAP-DF grants 00193.00001808/2022 − 71. This study was financed in part by the Coordenação de Aperfeiçoamento de Pessoal de Nível Superior - Brasil (CAPES) - Finance Code 88887.691997/2022-00. M.L.P.J and L.A.R.J. acknowledge CENAPAD-SP for providing computational facilities. L.A.R.J. gratefully acknowledges the support from ABIN grant 08/2019. A.M.F. gratefully acknowledges the support from Conselho Nacional de Desenvolvimento Científico (CNPq), grants 459961/2014 − 4 and 424950/2018 − 9.

Author Contributions D.A.F.M., K. A. L., and F.F.M.: data curation, formal analysis, methodology, and writing—original draft preparation. M.L.P.J.: data curation, formal analysis, methodology and, funding acquisition. L.A.R.J. and A.M.F.: conceptualization, funding acquisition, and writing—reviewing and editing. All authors reviewed the manuscript.

Funding Brazilian Research Councils FAP-DF, CNPq, and CAPES.

Data availability Not applicable.

Declarations

Ethical approval Not applicable.

Conflict of interest The authors declare no competing interests.

References

1. Bhimanapati GR, Lin Z, Meunier V, Jung Y, Cha J, Das S, Xiao D, Son Y, Strano MS, Cooper VR et al (2015) ACS nano 9(12):11509
2. Novoselov KS, Geim AK, Morozov SV, Jiang De, Zhang Y, Dubonos SV, Grigorieva IV, Firsov AA (2004) science 306(5696):666
3. Avouris P, Freitag M (2013) IEEE Journal of selected topics in quantum electronics 20(1):72
4. Zhang S, Zhou J, Wang Q, Chen X, Kawazoe Y, Jena P (2015) Proceedings of the National Academy of Sciences 112(8):2372
5. Wang Z, Zhou XF, Zhang X, Zhu Q, Dong H, Zhao M, Oganov AR (2015) Nano letters 15(9):6182
6. Li X, Wang Q, Jena P (2017) The journal of physical chemistry letters 8(14):3234
7. Wang S, Yang B, Chen H, Ruckenstein E (2018) Journal of Materials Chemistry A 6(16):6815
8. Chen JH, Autès G, Alem N, Gargiulo F, Gautam A, Linck M, Kisielowski C, Yazyev O, Louie S, Zettl A (2014) Physical Review B 89(12):121407
9. Fan Q, Yan L, Tripp MW, Krejčí O, Dimosthenous S, Kachel SR, Chen M, Foster AS, Koert U, Liljeroth P et al (2021) Science 372(6544):852
10. Hu Y, Wu C, Pan Q, Jin Y, Lyu R, Martinez V, Huang S, Wu J, Wayment LJ, Clark NA et al (2022) Nature Synthesis 1(6):449
11. Desyatkin VG, Martin WB, Aliev AE, Chapman NE, Fonseca AF, Galvão DS, Miller ER, Stone KH, Wang Z, Zakhidov D et al (2022) Journal of the American Chemical Society 144(39):17999
12. Toh CT, Zhang H, Lin J, Mayorov AS, Wang YP, Orofeo CM, Ferry DB, Andersen H, Kakenov N, Guo Z et al (2020) Nature 577(7789):199
13. Hou L, Cui X, Guan B, Wang S, Li R, Liu Y, Zhu D, Zheng J (2022) Nature 606(7914):507
14. Jana S, Bandyopadhyay A, Datta S, Bhattacharya D, Jana D (2021) Journal of Physics: Condensed Matter 34(5):053001
15. Sattar N, Sajid H, Tabassum S, Ayub K, Mahmood T, Gilani MA (2022) Science of The Total Environment 824:153858
16. Ashraf A, Herbert JM, Muhammad S, Farooqi BA, Farooq U, Salman M, Ayub K (2022) ACS omega 7(2):2260
17. Jadoon T, Ahsin A, Ullah F, Mahmood T, Ayub K (2021) Journal of Molecular Liquids 341:117415
18. Jadoon T, Mahmood T, Ayub K (2021) Journal of Physics and Chemistry of Solids 153:110028
19. Khan S, Sajid H, Ayub K, Mahmood T (2020) Journal of Molecular Liquids 316:113860
20. Popov MN, Dengg T, Gehringer D, Holec D (2020) C 6(2):20
21. Álvarez-Zapatero P, Herrero A, Lebon A, Gallego L, Vega A (2021) International Journal of Hydrogen Energy 46(29):15724
22. Kumar AVN, Prabhu SM, Shin WS, Yadav KK, Ahn Y, Abdellattif MH, Jeon BH (2022) Coordination Chemistry Reviews 467:214613
23. Kamran U, Park SJ (2021) Journal of Cleaner Production 290:125776
24. Ataca C, Ibrahim A, Bhattarai A (2023) Bulletin of the American Physical Society
25. Li C, Wang Y, Li C, Xu S, Hou X, Wu P (2019) ACS applied materials & interfaces 11(23):20770
26. Wang Z, Li P, Chen Y, Liu J, Zhang W, Guo Z, Dong M, Li Y (2015) Journal of Materials Chemistry C 3(24):6301
27. Chen Y, Liu Yj, Wang Hx, Zhao Jx, Cai Qh, Wang Xz, Ding Yh (2013) ACS applied materials & interfaces 5(13):5994
28. Huang K, Sun Y, Zhang Y, Wang X, Zhang W, Feng S (2019) Advanced Materials 31(38):1801430
29. Kim J, Park J, Lee J, Lim WG, Jo C, Lee J (2021) Advanced Functional Materials 31(22):2010882
30. Pendashteh A, Palma J, Anderson M, Marcilla R (2017) Applied Catalysis B: Environmental 201:241
31. Wang S (2011) Physical Chemistry Chemical Physics 13(25):11929
32. Mélinon P, Masenelli B, Tournus F, Perez A (2007) Nature materials 6(7):479
33. Georgakilas V, Perman JA, Tucek J, Zboril R (2015) Chemical reviews 115(11):4744
34. Singla M, Sharma D, Jaggi N (2021) International Journal of Hydrogen Energy 46(29):16188
35. Chen Y, Yang Xc, Liu Yj, Zhao Jx, Cai Qh, Wang Xz (2013) Journal of Molecular Graphics and Modelling 39:126
36. Kumar S, Sharma S, Karmaker R, Sinha D (2021) Materials Today Communications 26:101755
37. Salih E, Ayesh AI (2021) Materials Chemistry and Physics 267:124695
38. Tang Y, Yang Z, Dai X, Ma D, Fu Z (2013) The Journal of Physical Chemistry C 117(10):5258

39. Yuksel N, Kose A, Fellah MF (2022) Sensors and Actuators A: Physical 344:113726
40. Gong B, Wu H, Sheng L, Zhang W, Wu X (2022) ACS Applied Materials & Interfaces 14(11):13231
41. Esrafili MD, Saeidi N, Nematollahi P (2016) Chemical Physics Letters 658:146
42. Düzenli D (2016) The Journal of Physical Chemistry C 120(36):20149
43. Mao X, Kour G, Zhang L, He T, Wang S, Yan C, Zhu Z, Du A (2019) Catalysis Science & Technology 9(23):6800
44. Pullamsetty A, Subbiah M, Sundara R (2015) International journal of hydrogen energy 40(32):10251
45. Lee Y, Lee S, Hwang Y, Chung YC (2014) Applied surface science 289:445
46. Zou Y, Li F, Zhu Z, Zhao M, Xu X, Su X (2011) The European Physical Journal B 81:475
47. Zhu X, Liu K, Lu Z, Xu Y, Qi S, Zhang G (2020) Physica E: Low-dimensional Systems and Nanostructures 117:113827
48. Dai J, Yuan J, Giannozzi P (2009) Applied Physics Letters 95(23):232105
49. Grimme S (2006) Journal of computational chemistry 27(15):1787
50. Delley B (1990) The Journal of chemical physics 92(1):508
51. Andzelm J, Kölmel C, Klamt A (1995) The Journal of Chemical Physics 103(21):9312. https://doi.org/10.1063/1.469990
52. Delley B (2000) The Journal of chemical physics 113(18):7756
53. Kresse G, Joubert D (1999) Physical review b 59(3):1758
54. Perdew JP, Burke K, Ernzerhof M (1996) Physical review letters 77(18):3865
55. Perdew JP, Wang Y (1992) Physical review B 45(23):13244
56. Kohn W, Sham LJ (1965) Physical review 140(4A):A1133
57. Delley B (2002) Physical Review B 66(15):155125
58. Monkhorst HJ, Pack JD (1976) Physical review B 13(12):5188
59. Lima KAL, Cunha WFd, Monteiro FF, Enders BG, MLP Jr, LAR Jr (2019) Journal of Molecular Modeling 25:1
60. Paura ENC, da Cunha WF, de Oliveira Neto PH, e Silva GM, Martins JB, Gargano R (2013) The Journal of Physical Chemistry A 117(13):2854
61. Paura EN, da Cunha WF, Martins JBL, e Silva GM, Roncaratti LF, Gargano R (2014) Rsc Advances 4(54):28249
62. Lima IT, Gargano R, Guerini S, Paura EN (2019) New Journal of Chemistry 43(20):7778
63. Mananghaya MR (2020) Adsorption 26(3):461
64. Jiang T, Xiong R, Huang T, Li M, Zhang Y, Zhou H (2022) Diamond and Related Materials 130:109409
65. Sanyal B, Eriksson O, Jansson U, Grennberg H (2009) Physical Review B 79(11):113409
66. Timsorn K, Wongchoosuk C (2020) Materials Research Express 7(5):055005. https://doi.org/10.1088/2053-1591/ab8b8b
67. Peng S, Cho K, Qi P, Dai H (2004) Chemical Physics Letters 387(4):271. https://doi.org/10.1016/j.cplett.2004.02.026. http://www.sciencedirect.com/science/article/pii/S0009261404002398